

ELECTRONIC SUPPORTING INFORMATION.

Selective biomineralization of $\text{Co}_3(\text{PO}_4)_2$ -sponges triggered by His-tagged proteins; an efficient heterogeneous biocatalyst for redox processes.

Fernando López-Gallego^{a,b*}, Luis Yatea

^a*CIC BiomaGUNE, Pase Miramon 182, 20009, San Sebastian (Spain)*

^b*IKERBASQUE, Basque Foundation for Science, Bilbao (Spain)*

*flopez.ikerbasque@cicbiomagune.es

1. Materials

The genes of N-terminal His-tagged alcohol dehydrogenase from *Geobacillus stearothermophilus* and alcohol dehydrogenate from *Lactococcus lactis* were synthesized and cloned into pET28b(+) (pET28-*adh_bs* and pET28-*adh_ll*) by Eurofins (Hamburg, Germany). Cobalt chloride, PBS (10X), acetone, and ethanol were purchased from Sigma-Aldrich (St. Louis, IL). NAD^+ and NADH were purchased from GERBU Biotechnik GmbH (Wieblingen, Germany). TALON resin was purchased from Clontech (Saint-Germain-en-Laye, France).

2. Methods

Production of the recombinant *hisBs*-ADH and *hisLl*-ADH in *E.coli*: *E.coli* BL21 (DE3) cells were transformend with the recombinant plasmid pET28-*adh_bs*. These cells were cultivated at 37° C in LB medium containing 30 $\mu\text{g mL}^{-1}$ kanamycin. When the culture reached 0.6 O.D, 1-thio- β -d-galactorpyranoside (IPTG) was added up to 1 mM to induce the expression of *hisBs*-ADH. After induction the cell were grown for 3 h and collected by centrifugation (1699 rcf)

Purification of *hisBs*-ADH and *his-Ll*-ADH: For protein purification, we harvested the cells and then resuspended them in 25 mM sodium phosphate pH 7 (binding buffer). The suspension was sonicated, then the cell debris was removed by centrifugation and cleared crude extract was purified by metal affinity chromatography. Soluble protein was loaded on a Talon resin equilibrated with binding buffer. Following the protein binding to the column, we washed the column three times with binding buffer prior to the protein elution with elution buffer (binding buffer supplemented with 300 imidazol). The eluted protein was gel-filtered by using PD-10 columns (GE healthcare) to remove the imidazol and exchange the enzyme buffer to PBS 1X. The concentration of pure and gel-filtered protein was measured by using Bradford reagent (BioRad).

Synthesis of bio-inorganic sponges: In a typical experiment 6.6 μL of either 120 mM CuSO_4 or CoCl_2 solution was mixed with 1mL of 0.1 mg/mL *hisBs*-ADH in PBS. The reaction was incubated at different times. Control reactions mixing the metal salts and PBS (without His-tagged protein) were also carried out. The mineralization solutions were centrifuged (20817 rcf) and washed with 1mL of PBS for 3 times. For SEM analysis, the

samples were washed with pure water instead of PBS in order to remove unspecific phosphate crystals. Supernatant of the biomineralization solution was kept before the first wash in order to quantify both protein concentration and enzyme activity. After washing, the precipitate containing the bio-inorganic sponges was resuspended into 25 mM sodium phosphate at pH 7 and its enzyme activity was assayed. To carry out the mineralization with the untagged Bs-ADH, the enzyme was incubated with thrombin to remove the His-tag by protein digestion. The immobilization yield (Ψ) means the amount of soluble Bs-ADH incorporated to the biomineral and is defined as: $\Psi = (\text{protein concentration in the supernatant after 3 days biomineralization} / \text{initial protein concentration before adding the metal salt}) \times 100$. The Relative specific activity (RsA (%)) means the relative specific activity of Bs-ADH incorporated into the biomineral regarding to the specific activity (sA) of soluble Bs-ADH, and is defined as $\text{RsA}(\%) = (\text{sA}_{\text{biomineral}}(\text{U/mg}) / \text{sA}_{\text{soluble}}(\text{U/mg})) \times 100$. Finally, the biomineralization efficiency (η) means the fraction of Bs-ADH molecules that have been incorporated into the biomaterial in their active form and is defined as: $\eta = (\Psi \times \text{sA}) / 10000$. This parameter refers to both the immobilization capacity and the inactivation effect of the biomineralization technique.

Enzyme assay: The enzymatic activities were spectrophotometrically measured by monitoring the absorbance at 340 nm, which varied depending on the concomitant production or consumption of NADH. Generally, the reaction was carried out at 25 °C and pH7; however we studied the effect of both temperature and pH on the enzyme activity, so assay temperature and pH might change, in this case they are indicated in the experiment. For the reduction reaction, 190 μL of 105 mM acetone and 0.105 mM NADH in 25 mM sodium phosphate buffer were incubated with 10 μL of enzymatic solution (either soluble or immobilized). For the oxidation reaction, 190 μL of 105 mM 1,4 butanediol and 0.105 mM NADH in 25 mM sodium phosphate buffer were incubated with 10 μL of enzymatic solution (either soluble or immobilized). In the case of the Ll-ADH activity, we used phenylacetaldehyde as substrate and NADH consumption was monitored. One unit of activity was defined as the amount of enzyme that was needed to either reduced or oxidized 1 μmol of the corresponding nicotinamide cofactor at 340 nm, 25 °C and pH 7.

Kinetic parameters: Steady-steady kinetic of soluble and mineralized *his*Bs-ADH were determined by the enzyme assay varying concentrations of acetone (0.1-200 mM) and NADH (1-200 μM) at pH 7 and 25 °C. The data were adjusted to the Michaelis-Menten equation by using non-linear regression fitting.

Structural characterization of bio-inorganic sponges: The size and morphology of the bio-inorganic sponges were examined using the scatter detector of JEOL- JSM-6490LV, while determination of the atomic composition of the solid materials was carried out with Oxford Inca EDX system. Moreover, RAMAN spectroscopy of the solid samples was carried out with InVia Reflex Raman microscope from Renishaw. The RAMAN spectra were taken by exciting the sample with 633 nm laser. Finally, the solid particles were analyzed by XPS using a SPECS Sage HR 100 spectrometer with a non-monochromatic X-ray source (Aluminum $K\alpha$ line of 1486.6 eV energy) at 300 W and calibrated using the $3d_{5/2}$ line of Ag with a full width at half maximum (FWHM) of 1.2 eV. An electron flood gun was used to

compensate for charging during XPS data acquisition. The selected resolution for the high resolution spectra was 15 eV of Pass Energy and 0.15 eV/step. All Measurements were made in an ultra high vacuum (UHV) chamber at a pressure around $5 \cdot 10^{-8}$ mbar. The etching of the samples was done with an Ar^+ beam with energy of 3 kV at several times.

3. Supporting Results

Bio-mineralization of his-BsADH in presence of copper-phosphate. Biomineral of copper phosphate was spherical with an average size of 20 μm (**Figure S2**). Likewise previous nanoflowers reported for other enzyme, it showed a flower-like structure with petals but more spherical, more compacted and larger than the copper-phosphate nanoflowers observed for other untagged proteins

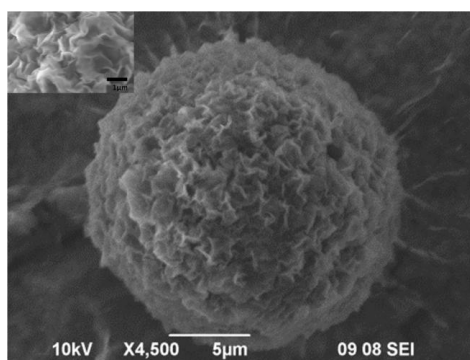


Figure S1. SEM images of $\text{Cu}_3(\text{PO}_4)_2$ -biosponges using Bs-ADH tagged with 6xHis at its N-terminus.

Inactivation of his-BsADH in presence of different divalent metals.

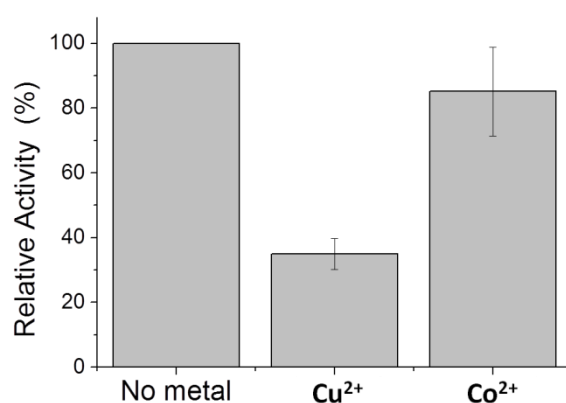


Figure S2. Inactivation of Bs-ADH in presence of different metals. 0.05 mg/mL Bs-ADH wer incubated for 15 minutes with 10 mM Tris-HCl buffer without metals and with 0.8 mM of either CuSO_4 or CoCl_2

Selective biomineralization of cobalt-phosphate triggered by His-tag. We incubated a protein crude extract overexpressing *hisBs*-ADH with cobalt chloride and PBS, resulting in the selective mineralization of the tagged protein rather than any other protein from the untagged pool (**Figure S3**). These data indicate that, unlike copper-minerals, His-tag drives the mineralization of cobalt-minerals, which agrees with the fact that Co^{2+} -chelates are much more selective for proteins tagged with His-cluster than Cu^{2+} -chelates that can unspecifically bind even untagged proteins. This higher selectivity relies on the lower affinity of Co^{2+} for proteins which explains that untagged proteins hardly induce the formation of $\text{Co}_3(\text{PO}_4)_2$ mineral particles.

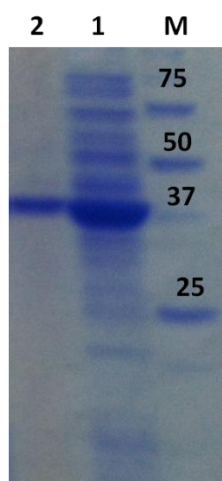


Figure S3. SDS-PAGE of selective biomineralization of Bs-ADH tagged with 6xHis at its N-terminus. Crude extract of BL21 overexpressing Bs-ADH with His-tag (line 1). Precipitate after the crude extract biomineralization (line 2). The crude extract was incubated with PBS and 0.8 mM CoCl_2 for three days. Then, the biomineral was collected by centrifugation and intensively washed with PBS to remove all not bound proteins. The right line (line M) indicates the molecular markers that help to identify the target protein.

Evolution of immobilization yield specific activity, size and colour of bio-inorganic sponges. We observed changes in both immobilization yield and relative specific activity of *hisBs*-ADH incorporated into the biominerals (**Figure S4A**) at different growth stages. Surprisingly, we observed a decreasing on the immobilization yield during the early stage of the growth, while immobilization yield was stable (around 55%) at the end of the biomineralization process. On the other hand, the specific activity of the enzyme incorporated into the bio-inorganic sponges decreased along the particle size was increased (**Figure S4**). We also noticed differences in colour based on the biomineralization stage; while the biominerals grown for 3 days showed a violet colour, the ones grown for 12 days were pink (**Figure S5**). These different colours suggest different hydration state of $\text{Co}_3(\text{PO}_4)_2$ salt.

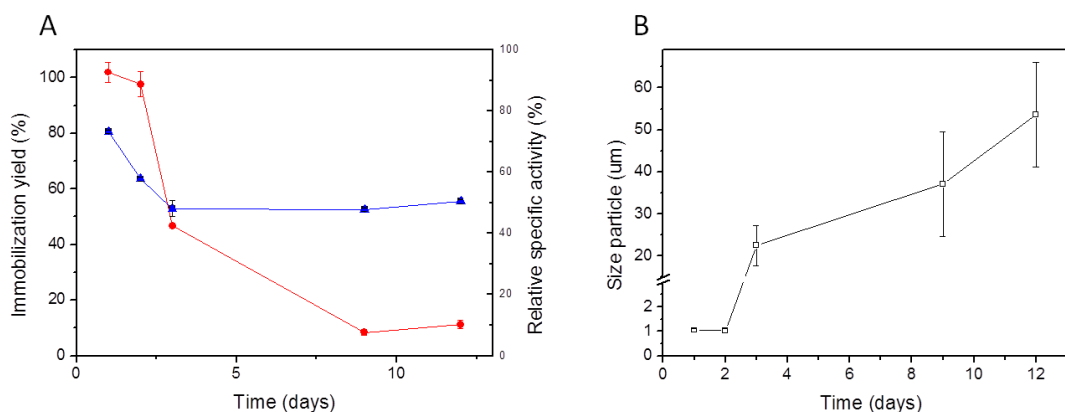


Figure S4. Time-course of different $\text{Co}_3(\text{PO}_4)_2$ -biomineralization parameters. (A) The protein immobilization yield (blue triangles) and the relative specific activity of the immobilized enzyme (red circles) were monitored along the biomineralization time. (B) The mean diameter of the resulting Bs-ADH bio-inorganic sponges at different times. The mean size values are the average of the diameters of 10 different particles.

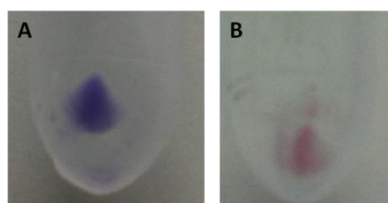


Figure S5. Precipitates resulting from biomineralization of $\text{Co}_3(\text{PO}_4)_2$ triggered by His-tagged Bs-ADH at different times. 3 days (A) and 12 days (B).

Physical characterization of bio-inorganic sponges by EDX and XPS . EDX analysis of cobalt-phosphate biosponges revealed the presence of N and the higher C/O ratio (**Figure S6 and 7**). Moreover, EDX maps also showed the uniform distribution of N, P and Co across the same particle that corroborates the co-localization of both protein and inorganic salts. Contrarily, precipitation of $\text{Co}_3(\text{PO}_4)_2$ in absence of the His-tagged protein formed large crystals where N could not be detected and their C/O ratio was rather low compared to the bio-inorganic sponges (**Figure S7**). We also carried out the EDX analysis at higher acceleration voltage (**Figure 7D and F**) to determine the atomic composition at deeper layers of the materials we detected higher intensity of cobalt signal, which was uniformly distributed across the particle. This experimental evidence suggests that proteins were uniformly occupying the first surface layer of these particles. To confirm this idea, we analyzed the bio-inorganic sponges with XPS at different depths, confirming the presence of Co^{2+} according to the peak shape and position in the Co 2p spectrum (**Figure S8A**), and more interestingly that the deeper we measured, the higher cobalt and lower nitrogen contents were detected (**Figure S8B**). It seems that the protein localization at the surface hinders the cobalt signal in both XPS without etching and EDX with low acceleration voltage.

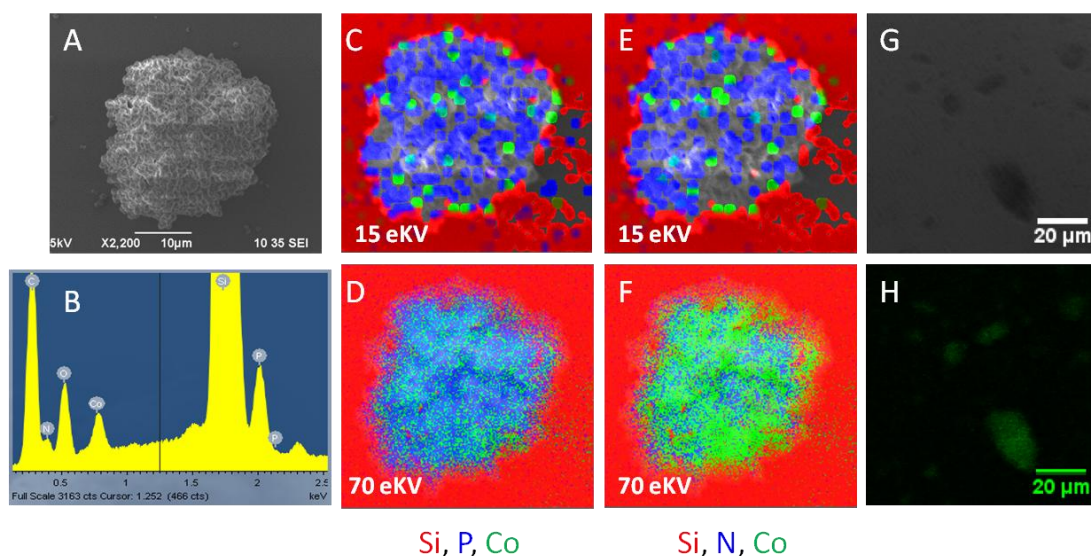


Figure S6. SEM images and EDX analysis of Bs-ADH/Co₃(PO₄)₂ sponges. SEM images of Bs-ADH bio-inorganic sponges. Elemental analysis of Co₃(PO₄)₂ mineral by EDX (B). EDX maps of one particle of Co₃(PO₄)₂ mineral detecting (C, D) Si (red), P (blue) and Co (green) and detecting (E, F) Si (red), carbon (blue) and Co (green). EDX was carried out at different acceleration voltages, 15 eKV (C, E) and 70 eKV (E, F). Confocal laser microscopy images, bright field (G) and fluorescence of His-GFP (H).

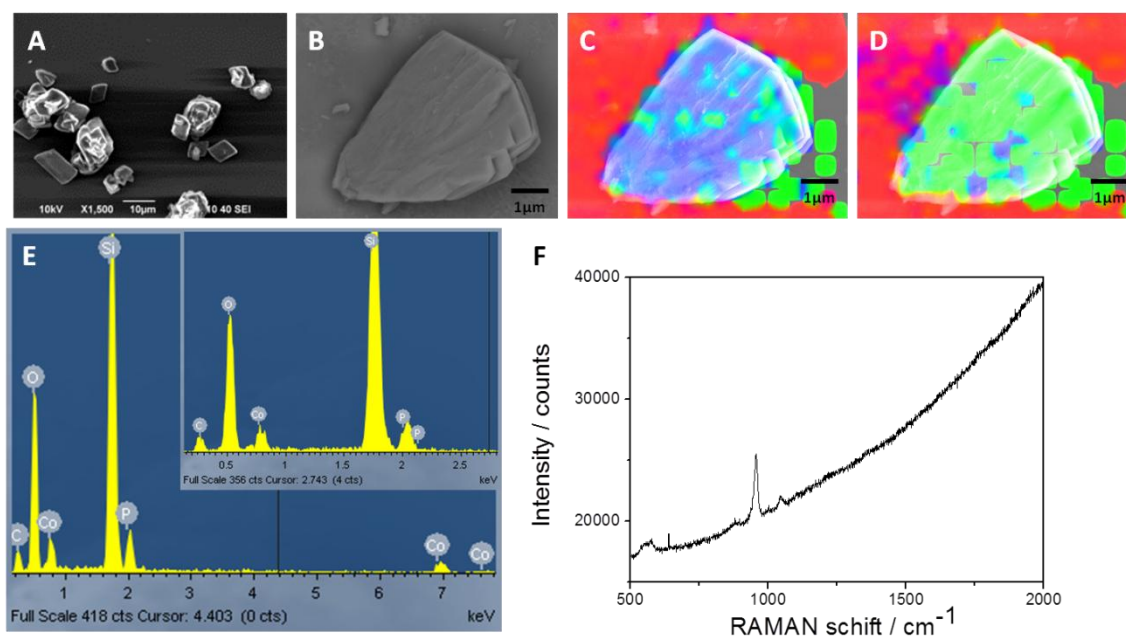


Figure S7. SEM images, EDX and RAMAN analysis of control Co₃(PO₄)₂ minerals. SEM images of Co₃(PO₄)₂ minerals low (A) and high magnification (B). EDX maps of one particle of Co₃(PO₄)₂ mineral detecting (C) Si (red), P (blue) and Co (green) and detecting (D) Si (red), carbon (blue) and Co (green). Elemental analysis of Co₃(PO₄)₂ mineral by EDX (E). RAMAN spectrum of Co₃(PO₄)₂ mineral (F).

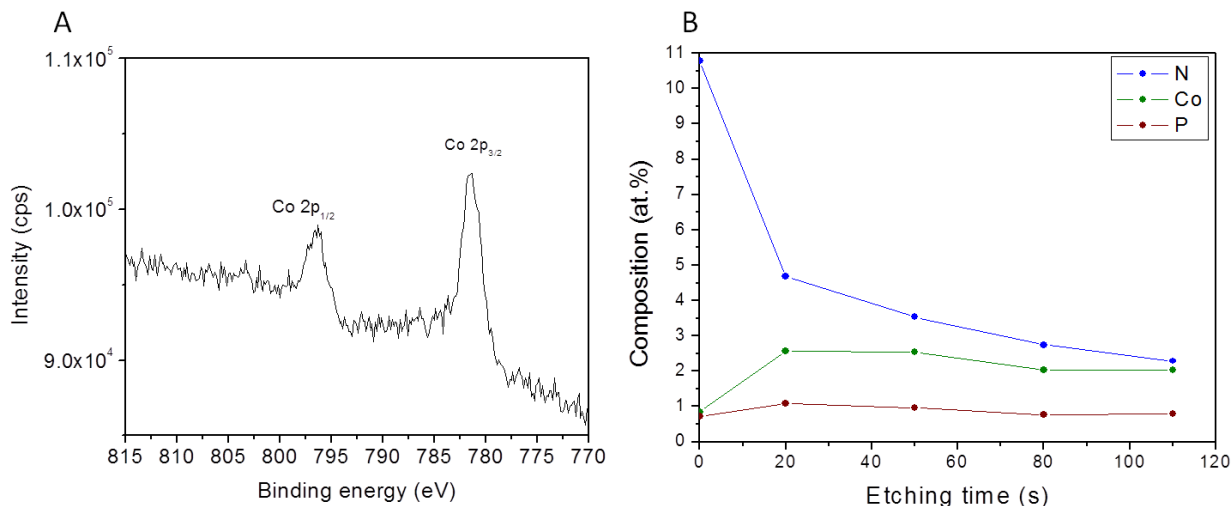


Figure S8. XPS analysis of Bs-ADH/Co₃(PO₄)₂ sponges. (A) This figure shows the high resolution spectrum of Co 2p peak without etching. (B) This plot represents the atomic composition of the sample at different etching times, indicating the nitrogen belonging to the protein is more abundant at the surface of the particles, while the Cobalt occupies deeper layers in the particles.

Thermal stability of soluble and mineralized his-BsADH

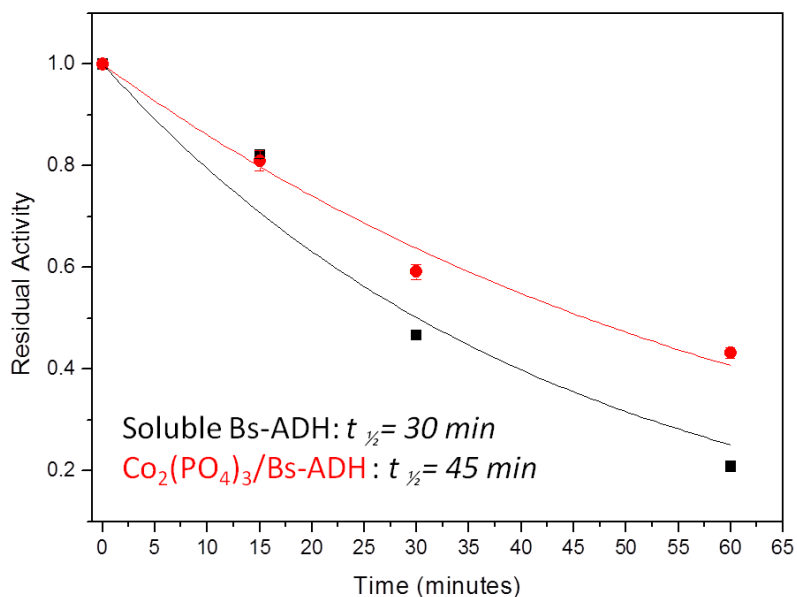


Figure S9. Thermal inactivation of soluble (black squares) and bio-inorganic sponges (red circles) of His-tagged Bs-ADH. The thermal inactivation was carried out at 70 °C, samples were withdrawn at different times and their enzymatic activity was assayed. The half-life times for each enzymatic preparation are indicated in the graph.

Kinetic parameters of bio-inorganic sponges. We studied the kinetic parameters for the reduction of acetone to isopropanol catalyzed by either the optimal bio-inorganic sponges or the soluble *hisBs*-ADH.

Table S1. Kinetic parameters of soluble and mineralized *his*-BsADH

Substrate	His-BsADH	K_M (mM)	k_{cat} (s^{-1})	K_{cat}/K_M ($M*s^{-1}$) x 10^3
NADH	Soluble	0.3±0.1	2.14±0.57	7.13
	Bio-inorganic sponge	0.19±0.03	1.48±0.15	7.8
Acetone	Soluble	2.28±1.40	0.47±0.05	0.2
	Bio-inorganic sponge	9.8±3.8	0.51±0.05	0.052

Catalytic applications of bio-inorganic sponges.

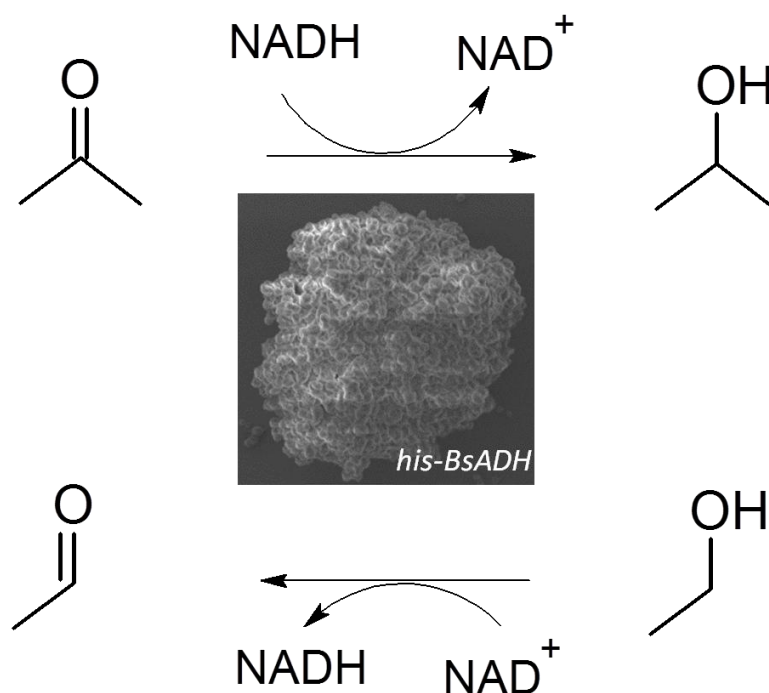


Figure S10. Redox reaction catalyzed by bio-inorganic sponges. Bioreduction of acetone to isopropanol by using NADH as redox cofactor, and oxidation of ethanol to acetaldehyde by using NAD⁺ as cofactor.